Instability of uniform turbulent plane Couette flow: spectra, probability distribution functions and $K - \Omega$ closure model

Laurette S. Tuckerman, Dwight Barkley and Olivier Dauchot

Abstract Near transition, plane Couette flow exhibits statistically steady bands of alternating turbulent and laminar flow. We simulate these patterns numerically and show that they can be quantified via the spatial Fourier component corresponding to the pattern wavevector and its probability distribution. The trigonometric nature of the turbulent-laminar pattern suggests that it emerges from a linear instability of the uniform turbulent state, and we attempt to verify this hypothesis via the $K - \Omega$ closure model. We calculate steady 1D solution profiles of the $K - \Omega$ model and their linear stability to 3D perturbations, but find no correspondence between this analysis and the onset of turbulent-laminar bands in experiment and simulation.

1 Turbulent-laminar bands

Near transition, plane Couette flow exhibits a remarkable statistically steady state containing alternating oblique bands of turbulent and laminar flow which are regular and statistically steady. Discovered experimentally by Prigent and Dauchot (GIT-Saclay) [1, 2] and subsequently simulated numerically by Barkley and Tuckerman [3, 4, 5, 6], these patterns seem to be an intrinsic feature of the transition to turbulence in shear flows, since they are also seen experimentally in counter-rotating Taylor-Couette flow [1, 2] and the stator-rotor configuration [7], as well as in simulations of plane Poiseuille flow [8], and pipe flow [9].

Laurette S. Tuckerman
PMMH-ESPCI (UMR 7636, CNRS, Univ. Paris 6 & 7), 10 rue Vauquelin, 75231 Paris, France, e-mail: laurette@pmmh.espci.fr

Dwight Barkley
Mathematics Institute, Univ. Warwick, United Kingdom, e-mail: D.Barkley@warwick.ac.uk

Olivier Dauchot
CEA-Saclay, SPEC-GIT, URA 2464, 91191 Gif-sur-Yvette, France, e-mail: dauchot@cea.fr

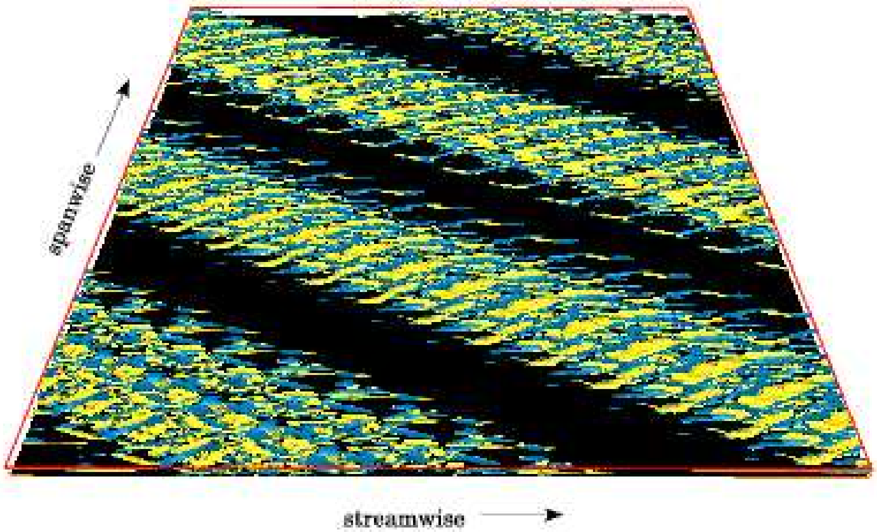

Fig. 1 Turbulent-laminar pattern at Reynolds number 350. Isosurfaces of instantaneous streamwise vorticity. This visualization is constructed by tiling a large domain with many repetitions of our computational domain.

Figure 1 shows a perspective plot of a turbulent-laminar patterned flow computed by our simulations at $Re = 350$. The upper and lower plates are located at $\pm h$ and move in the streamwise direction at $\pm U$; the conventional Reynolds number is Uh/ν. In the flow of figure 1, the width of the bands is 40 in units of h, and they are oriented at an angle of $\theta = 24^\circ$ from the streamwise direction, so that the pattern wavevector is oriented at 66°. This width and angle are within the typical range of these patterns [1, 2].

We focus on the transition from uniform turbulence to turbulent-laminar patterns with decreasing Reynolds number, which takes place near $Re = 400$. This low Reynolds number is quite accessible to direct numerical simulation of the Navier-Stokes equations. We first describe three numerically computed flows spanning the transition region, and characterize these flows by means of their Fourier transforms along the pattern wavevector.

Our simulations were carried out with the spectral-element/Fourier code `Prism` [10]. We use between 8 and 20 modes per unit length, leading to a resolution of about 10^6 gridpoints or modes. More details concerning our numerical methods can be found in [3, 4, 5, 6].

2 Analysis of Fourier spectra

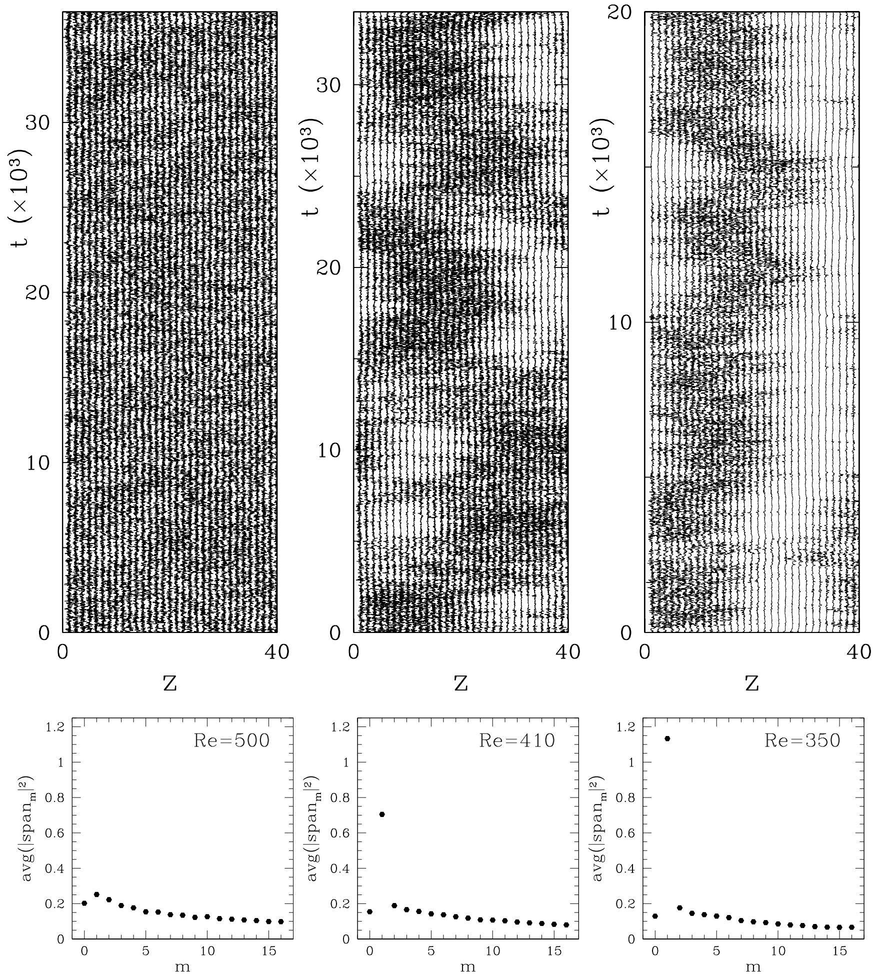

Fig. 2 Top row: timeseries of the spanwise velocity at 32 points along a line midway between the plates and oriented along the pattern wavevector. Bottom row: time-average of the power spectrum along the pattern wavevector of the spanwise velocity. The $m = 1$ component corresponds to the pattern wavelength of 40. Left column: uniform turbulence at $Re = 500$. Middle column: intermittent state at $Re = 410$. Right column: statistically steady turbulent-laminar pattern at $Re = 350$.

We now describe the onset of these patterns as the Reynolds number is decreased. The upper portion of figure 2 shows timeseries of the spanwise velocity for 32 points along a line located midway between the plates and oriented in the direction of the pattern wavevector. (In this figure, as in some of our previous work [4, 5, 6], z denotes the direction of the pattern wavevector, but in section 3 we will use z to denote the spanwise direction instead.)

Figure 2 shows that the turbulence is *uniform* for $Re = 500$ and *banded* for $Re = 350$. At the intermediate value $Re = 410$, the turbulence is *intermittent*, with a pattern appearing and disappearing sporadically. We then process this data by taking the square modulus of the Fourier transform along the pattern wavevector $|\text{span}_m(t)|^2$ at each instant t, and then averaging over time for each Re. This yields the 1D power spectra $\underset{t}{\text{avg}}\, |\text{span}_m(t)|^2)$ of the spanwise velocity, shown in the lower portion of figure 2. These spectra display a very prominent feature: the $m = 1$ Fourier component corresponding to wavelength 40 emerges from the rest of the spectrum at $Re = 350$ and, to a lesser extent, at $Re = 410$. The emergence of the $m = 1$ Fourier component suggests using it as an order parameter for the transition from uniform to banded turbulence, as shown in figure 3.

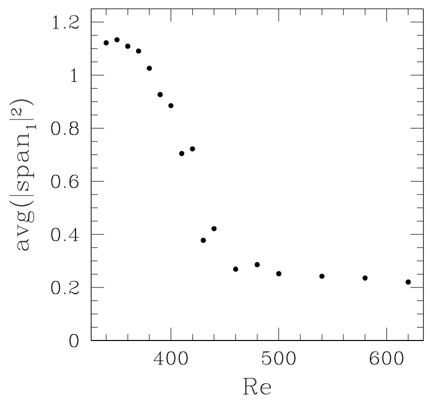

Fig. 3 Bifurcation diagram for transition from uniform to banded turbulence using $m = 1$ component of averaged power spectra, as in figure 2.

To obtain a sharp threshold, however, it is necessary to return to the instantaneous component $a(t) \equiv |\text{span}_1(t)|$. Rather than averaging these over time, we treat the instantaneous values as statistical samples and, by binning these, construct their probability distribution function $p(a)$. The resulting probability distribution functions for $Re = 500$, 410 and 350 are shown in figure 4. We can distinguish different regimes: For $Re \gtrsim 440$, the most probable value of a is zero, and this is where $p(a)$ has its maximum. At $Re = 440$, $p(a)$ changes curvature and, for $Re \lesssim 440$, $p(a)$ has a local minimum at $a = 0$ and a maximum at a finite value $a_{\max} > 0$.

Although a Gaussian provides an extremely good fit to $p(a)$ for $Re = 500$, the functional form which best fits $p(a)$ for $Re = 410$ and 350 as well is:

$$\ln p(a) = c_0 + c_1 a + c_2 a^2 \tag{1}$$

rather than the more usual quartic. The functional form (1) gives $a_{\max} = -c_1/(2c_2)$ as the most probable value. Both $a_{\max}$ and c_1 are shown on the right part of figure 4.

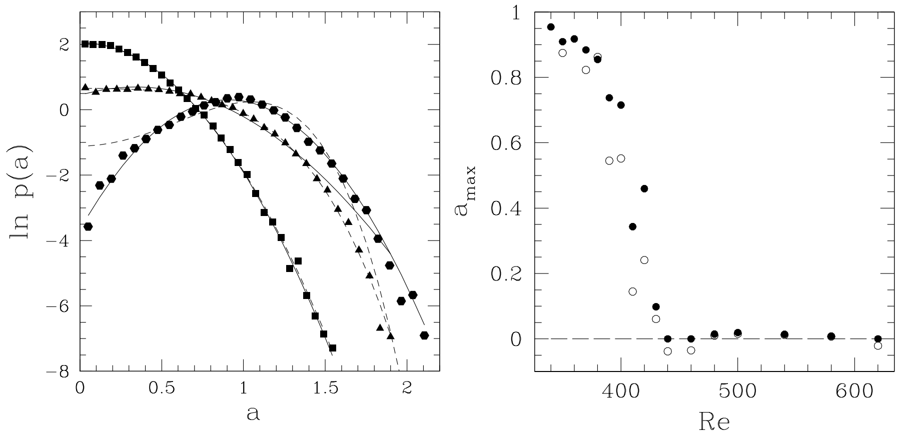

Fig. 4 Left: probability distribution functions $p(a)$ for pattern Fourier component. $Re = 500$ (squares), $Re = 410$ (triangles), and $Re = 350$ (circles). Solid curves are least-squares fits to $\ln p(a) = c_0 + c_1 a + c_2 a^2$, dashed curves to $\ln p(a) = c_0 + c_2 a^2 + c_4 a^4$, Right: maximum $a_{\max}$ of PDFs as a function of Reynolds number (solid dots) and coefficient $c_1/10$ (hollow dots) from least-squares fit.

3 Stability analysis of $K-\Omega$ Model

The sequence seen in figures 2-4, in particular the emergence of a single trigonometric mode, suggests that these patterns result from a linear instability of the *uniform turbulent state*, whose temporal average depends only on a single spatial variable: the cross-channel coordinate y.

We decompose the velocity field into its *short-time* mean and its fluctuating parts:

$$\mathbf{U} = \bar{\mathbf{U}} + \mathbf{U}' \qquad \text{where } \bar{\mathbf{U}} \equiv \langle \mathbf{U} \rangle \quad \text{and } \langle \mathbf{U}' \rangle = 0 \tag{2}$$

$\bar{\mathbf{U}}$ is governed by the Reynolds-averaged equations:

$$\partial_t \bar{\mathbf{U}} = -\nabla P - (\bar{\mathbf{U}} \cdot \nabla)\bar{\mathbf{U}} + \mathbf{F} + \frac{1}{Re}\Delta\bar{\mathbf{U}} \tag{3a}$$

$$\nabla \cdot \bar{\mathbf{U}} = 0 \tag{3b}$$

where the Reynolds stress force is $\mathbf{F} \equiv -\langle (\mathbf{U}' \cdot \nabla)\,\mathbf{U}' \rangle$. These are subject to the boundary conditions which define plane Couette flow:

$$\bar{\mathbf{U}}(x, y = \pm 1, z) = \pm \mathbf{e}_x \tag{3c}$$

$$\bar{\mathbf{U}}(x + \lambda_x, y, z) = \bar{\mathbf{U}}(x, y, z + \lambda_z) = \bar{\mathbf{U}}(x, y, z) \tag{3d}$$

where x, y, z are the streamwise, cross-channel and spanwise directions, respectively.

Since (3a) contains the Reynolds stress force, which in turn depends on the fluctuations $\mathbf{U}'$ which we seek to bypass, we require a *closure model* relating $\mathbf{F}$ directly to the mean flow $\overline{\mathbf{U}}$. The $K-\Omega$ model, as described in [11, 12, 13] is that thought best adapted to walls and to low Reynolds numbers. Equations (3) are closed by approximating $\mathbf{F}$ as:

$$\mathbf{F} = \nabla\cdot(\nu_T 2\underline{\underline{S}}) \qquad \nu_T \equiv \frac{K}{\Omega} \qquad 2S_{ij} \equiv \partial_i U_j + \partial_j U_i \tag{4a}$$

where K and Ω are scalar fields which evolve according to:

$$\partial_t K = -\overline{\mathbf{U}}\cdot\nabla K + \nu_T S^2 - \beta^*(\Omega K) + \nabla\cdot\left(\left(\nu + \frac{\nu_T}{\sigma_K}\right)\nabla K\right) \tag{4b}$$

$$\partial_t \Omega = -\overline{\mathbf{U}}\cdot\nabla\Omega + \alpha S^2 - \beta\Omega^2 + \nabla\cdot\left(\left(\nu + \frac{\nu_T}{\sigma_\Omega}\right)\nabla\Omega\right) \tag{4c}$$

with typical parameters of $\alpha = 5/9$, $\beta = 3/40$, $\beta^* = 9/100$, $\sigma_K = \sigma_\Omega = 2$. K is to be interpreted as the kinetic energy density and has boundary conditions:

$$K(x, y = \pm 1, z) = 0 \tag{4d}$$

Ω is meant to account for the presence of the boundary and is subject to various phenomenological boundary conditions, such as:

$$\Omega(x, y = \pm 1, z) = 1/(\Delta y)^2 \tag{4e}$$

where Δy is the numerical grid spacing at the boundary.

We have computed steady 1D solutions of (3)–(4) for various Reynolds numbers. To do so, we set $\overline{\mathbf{U}}(x,y,z) = \overline{U}(y)\mathbf{e_x}$ and $\partial_t = \partial_x = \partial_z = 0$. We discretized the y direction over a grid of $N_y + 1 = 61$ points with a Chebyshev spacing $y_j = \cos j\pi/N_y$, which concentrates points at the boundaries, We then solved for $\overline{U}(y)$, $K(y)$ and $\Omega(y)$ via Newton's method. The left portion of figure 5 shows $\overline{U}$, K, and Ω profiles for $Re = 100$, 300 and 500, while the right portion compares $\overline{U}(y) - y$ to the averaged turbulent profiles from our full 3D simulations at $Re = 500$. Like [14], we find that the $K-\Omega$ model exhibits a bifurcation from laminar flow ($K = 0$, $U(y) = y$) to turbulent flow ($K > 0$)) at $Re \approx 100$, illustrated in the left portion of figure 6. (This is already inconsistent with actual plane Couette flow, in which the lowest Re at which turbulence has ever been observed is 220 in certain numerical simulations [4, 15] and more typically above 300 [3, 16].) For $Re = 300$ and 500, the U profiles have S-shapes and the K profiles show flattening in the bulk, both features found in actual turbulent channel flows.

We then carried out linear stability analysis by substituting

$$\left\{\begin{matrix} \overline{U}(y)\mathbf{e_x} \\ K(y) \\ \Omega(y) \end{matrix}\right\} + \left\{\begin{matrix} \overline{\mathbf{u}} \\ k \\ \omega \end{matrix}\right\} e^{\sigma t + 2\pi i(x/\lambda_x + z/\lambda_z)} \tag{5}$$

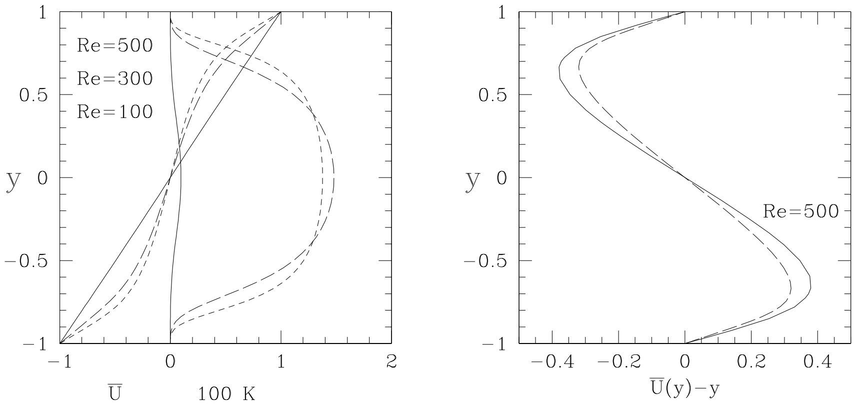

Fig. 5 Profiles from $K-\Omega$ model. Left: $Re = 100$ (solid curves), $Re = 300$ (long-dashed curves) and $Re = 500$ (short-dashed curves). $\overline{U}(y)$ ranges between -1 and $+1$, $K(y)$ has a bulge in the center. $\Omega(y)$ (not shown) is $O(10^6)$ at boundaries and decreases sharply to $O(1)$ in the bulk.
Right: comparison of $U(y)-y$ between $K-\Omega$ and full DNS. Solid and dashed curves show DNS and $K-\Omega$ profiles, respectively, for $Re = 500$.

into the full 3D equations (3)–(4), linearizing, and calculating the eigenvalues σ. In the ranges $90 \leq Re \leq 500$ and $10 \leq \lambda_x, \lambda_z \leq 1000$, we find that the eigenvalues $\sigma(\lambda_x, \lambda_z, Re)$ are all negative. The table on the right of figure 6 shows the maximum σ for each Re, maximized over the wavelengths λ_x, λ_z.

The largest (least stable) eigenvalue is found for $Re = 120$ at $(\lambda_x, \lambda_z) = (60, 20)$. This corresponds to a pattern angle of $\theta = \mathrm{atan}(\lambda_z/\lambda_x) = 18^\circ$ to the streamwise direction and a pattern wavelength of $\lambda_z \cos(\theta) = 19$. (see the Appendix of [5]). In contrast, turbulent-laminar patterns in plane Couette flow are observed experimentally at $300 \leq Re \leq 420$ with $\lambda_x = 110$ and $50 \leq \lambda_z \leq 80$, corresponding to an angle between 25° and 37° and a pattern wavelength of between 46 and 60. It is therefore unlikely that the instability of the $K-\Omega$ model bears any relationship to that undergone by uniform turbulent flow in plane Couette flow. A similar calculation using the simpler Prandtl mixing-length model also shows no instabilities.

This analysis underscores the inadequacy of turbulence closure models, in particular for transitional wall-bounded flows at low Reynolds numbers. Quantitative prediction of turbulent-laminar banded patterns would provide an extremely stringent test of a future closure model.

References

1. Prigent, A., Grégoire, G., Chaté, H., Dauchot, O., van Saarloos, W.: Large-scale finite-wavelength modulation within turbulent shear flows. Phys. Rev. Lett. **89**, 014501 (2002)

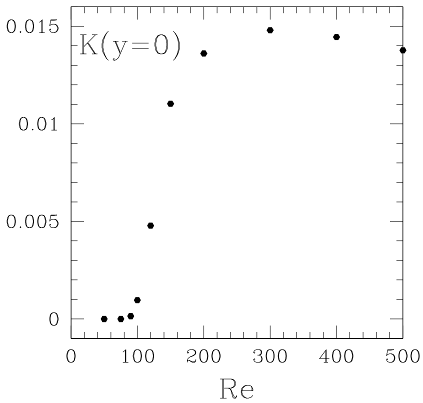

Re	λ_x	λ_z	σ
90	1000	500	−0.0179
100	90	30	−0.0190
110	60	20	−0.0135
120	60	20	−0.0081
150	100	30	−0.0181
200	500	1000	−0.0148
300	500	1000	−0.0141
400	500	1000	−0.0964
500	400	1000	−0.0855

Fig. 6 1D and 3D instabilities of the $K-\Omega$ model. Left: Steady 1D solution to the $K-\Omega$ model as a function of *Re*. Shown is $K(0)$, the turbulent kinetic energy in channel center. A bifurcation from the laminar state $K=0$ is seen at $Re \approx 100$. Right: Leading eigenvalues from 3D linear stability analysis of steady 1D solution. Shown is the maximum eigenvalue for each *Re*, varying $10 \leq \lambda_x, \lambda_z \leq 1000$.

2. Prigent, A., Grégoire, G., Chaté, H., Dauchot, O.: Long-wavelength modulation of turbulent shear flows. Physica D **174**, 100–113 (2003)
3. Barkley, D., Tuckerman, L.S.: Computational study of turbulent laminar patterns in Couette flow. Phys. Rev. Lett. **94**, 014502 (2005)
4. Barkley, D., Tuckerman, L.S.: Turbulent-laminar patterns in plane Couette flow. In: Mullin, T., Kerswell, R. (eds.) IUTAM Symposium on Laminar-Turbulent Transition and Finite Amplitude Solutions, pp. 107–127. Springer (2005)
5. Barkley, D., Tuckerman, L.S.: Mean flow of turbulent-laminar patterns in plane Couette flow. J. Fluid Mech. **576**, 109–137 (2007)
6. Tuckerman, L.S., Barkley, D., Dauchot, O.: Statistical analysis of the transition to turbulent-laminar banded patterns in plane Couette flow. J. Phys.: Conf. Ser. **137**, 012029 (2008)
7. Cros, A., Le Gal,P.: Phys. Fluids **14**, 3755–3765 (2002)
8. Tsukahara, T., Seki, Y., Kawamura, H., Tochio, D.: DNS of turbulent channel flow at very low Reynolds numbers. In Proc. 4th Int. Symp. on Turbulence and Shear Flow Phenomena, pp. 935–940 (2005)
9. Moxey, D., Barkley, D., to be published
10. Henderson, R.D., Karniadakis, G.E.: Unstructured spectral element methods for simulation of turbulent flows. J. Comput. Phys. **122**, 191–217 (1995)
11. Menter, F.R.: Two-equation eddy-viscosity turbulence models for engineering applications. AIAA Journal **32**, 1598–1609 (1994)
12. Durbin, P.A., Pettersson Reif, B.A.: Statistical Theory and Modeling for Turbulent Flows. Wiley (2001)
13. Wilcox, D.C.: Re-assessment of the scale-determining equation for advanced turbulence models, AIAA Journal **26**, 1414–1421 (1988)
14. Templeton, J.: Stability Analysis of the k-omega Turbulence Model for Channel Flow. Stanford University, 5 June 2000.
15. Schmiegel, A., Eckhardt, B.: Persistent turbulence in annealed plane Couette flow, Phys. Fluids **51**, 395–400 (2000).
16. Bottin, S., Daviaud, F., Manneville, P., Dauchot, O.: Discontinuous transition to spatiotemporal intermittency in plane Couette flow, Europhys. Lett. **43**, 171–176 (1998).